# Strong-coupling approach to the Mott-Hubbard insulator on a Bethe lattice in dynamical mean-field theory

Daniel Ruhl and Florian Gebhard
*Department of Physics, Philipps-Universität D-35032 Marburg, Germany*
(Received 21 September 2010; revised manuscript received 12 November 2010; published 19 January 2011)

We calculate the Hubbard bands for the half-filled Hubbard model on a Bethe lattice with an infinite coordination number up to and including third order in the inverse Hubbard interaction. We employ the Kato-Takahashi perturbation theory to solve the self-consistency equation of the dynamical mean-field theory analytically for the single-impurity Anderson model in multichain geometry. The weight of the secondary Hubbard sub-bands is of fourth order so that the two-chain geometry is sufficient for our study. Our results for the Mott-Hubbard gap and the density of states of the lower Hubbard band agree very well with those from numerical dynamical density-matrix renormalization group calculations, apart from a resonance contribution at the upper band edge, which cannot be reproduced in low-order perturbation theory.

DOI: 10.1103/PhysRevB.83.035120 PACS number(s): 71.10.Fd, 71.27.+a, 71.30.+h

## I. INTRODUCTION

The dynamical mean-field theory (DMFT) maps lattice models for electrons with a Hubbard-type interaction onto effective single-impurity models; for a review, see Ref. 1. The parameters of the impurity model must be determined in such a way that the self-energy and the Green function of the impurity model agree with the local self-energy and the local Green function of the lattice model. The solution of this self-consistency problem equally solves the original lattice problem in the limit of infinite dimensions.[2] For example, the Hubbard model on a Bethe lattice with an infinite coordination number can be mapped onto the single-impurity Anderson model (SIAM). Then, the self-consistency condition requires that its hybridization function and its Green function agree for all frequencies.

Unfortunately, we are far from an analytical solution of the SIAM for a general hybridization function, and a variety of methods have been employed to solve the DMFT equations for the single-band Hubbard model. Examples for numerical treatments are the numerical renormalization group method,[3] exact diagonalization,[4–6] the random dispersion approximation,[6,7] the dynamical density-matrix renormalization group (DDMRG) method,[6,8,9] and, at finite temperatures, quantum Monte Carlo (QMC).[10–12] Approximate analytical methods at zero temperature include the iterated perturbation theory,[13] the local-moment approach,[14] and the self-energy functional approach.[15]

All methods have their merits and limitations, and it is desirable to compare their results with those from perturbation theory. For the half-filled Hubbard model on a Bethe lattice with an infinite coordination number, the self-energy[16] and the ground-state energy[17] are known up to and including fourth order in the Hubbard interaction $U$ and up to second order in $1/U$.[6] However, these calculations are based on the Hubbard model in infinite dimensions not on the DMFT description.

In this paper, we solve the DMFT equations for the Hubbard model analytically on a Bethe lattice with an infinite coordination number, $Z \to \infty$, at half-band filling for strong coupling where the model describes a paramagnetic Mott-Hubbard insulator. Up to and including third order in $1/U$, we determine the hybridization function of the SIAM, which corresponds to the Hubbard model on the $Z \to \infty$ Bethe lattice. Essential to our approach are: (i) the mapping of the SIAM from the star geometry onto the multichain geometry where each chain represents one of the upper and lower Hubbard (sub-)bands; (ii) the Kato-Takahashi perturbation theory[18,19] for degenerate ground states; (iii) the Lanczos representation of the hybridization function and the Green function, which permits an order-by-order solution of the self-consistency equation for the moments of the density of states; (iv) the locality of the Hubbard interaction and of the Lanczos operators in finite-order perturbation theory.

Our paper is organized as follows. In Sec. II, we introduce the Hubbard model, the SIAM, the DMFT equations, and the two-chain mapping, which we use for our perturbative calculations for third order in $1/U$. In Sec. III, we adapt the Kato-Takahashi perturbation theory and use the Lanczos algorithm to express the density of states for the lower Hubbard band (LHB) and for the hybridization function in terms of their moments. Then, the self-consistency equation reduces to the condition that the respective moments agree up to trivial signs. In Sec. IV, we investigate the lowest nontrivial order and show how the iterative solution of the DMFT equation works in practice. Next, we summarize the results for third order; all technical details can be found in Ref. 20. The remaining problem is the calculation of the density of states at the boundary of a semi-infinite chain for a single particle, which can move between nearest neighbors and experiences a local potential at and near the boundary. Its solution and a favorable comparison with previous numerical work[8,11] is the subject of Sec. V. Conclusions, Sec. VI, close our presentation.

## II. MOTT-HUBBARD INSULATOR IN DYNAMICAL MEAN-FIELD THEORY

We start our presentation with the definition of the Hubbard model and the SIAM. For a specific choice of the hybridization function in the SIAM, its single-particle Green function is identical to the local single-particle Green function of the Hubbard model in infinite dimensions. The DMFT prescribes a way to determine the hybridization function self-consistently.

 

In general, the single-particle Green function for the SIAM cannot be calculated analytically. For the Mott-Hubbard insulator, we use a mapping of the model onto a multichain geometry where the chains represent the energy levels in the energetically separated upper and lower Hubbard (sub-)bands.

### A. Hamilton operators and Green functions

#### 1. Hubbard model

We consider the repulsive single-band Hubbard model ($U \geqslant 0$),

$$\hat{H} = \sum_{i,j;\sigma} t_{ij}\hat{c}^{\dagger}_{i,\sigma}\hat{c}_{j,\sigma} + U\sum_{i}\hat{n}_{i,\uparrow}\hat{n}_{i,\downarrow} - \mu\sum_{i}(\hat{n}_{i,\uparrow}+\hat{n}_{i,\downarrow}) =: \hat{T} + U\hat{D} - \mu\hat{N}. \tag{1}$$

Here, $\hat{T}$ denotes the operator for electron transfer between the lattice sites, the fermion operator $\hat{c}^{\dagger}_{i,\sigma}$ ($\hat{c}_{i,\sigma}$) creates (annihilates) an electron with spin $\sigma$ ($=\uparrow,\downarrow$) on lattice site $i$, the operator $\hat{n}_{i,\sigma} = \hat{c}^{\dagger}_{i,\sigma}\hat{c}_{i,\sigma}$ counts the number of $\sigma$ electrons on site $i$, and the operator $\hat{D} = \sum_i \hat{n}_{i,\uparrow}\hat{n}_{i,\downarrow}$ counts the number of doubly occupied sites. For the description of the Mott-Hubbard insulator, we consider a half-filled system where there is, on average, one electron per lattice site, $n = N/L = 1$. Moreover, we treat the paramagnetic situation, $n_{\uparrow} = n_{\downarrow} = 1/2$, without any symmetry breaking. The thermodynamic limit $N, L \to \infty$ is implicit in our following calculations.

As a major simplification, we assume that the electrons move between nearest neighbors on a Bethe lattice with coordination number $Z$,

$$t_{ij} = \begin{cases} -t/\sqrt{Z}, & \text{if } i,j \text{ are nearest neighbors,} \\ 0, & \text{else.} \end{cases} \tag{2}$$

Later, we will let go of $Z \to \infty$ and will choose $t = 1$ as our unit of energy. The Bethe lattice with coordination number $Z$ is an infinite $Z$-Cayley tree. A $Z$-Cayley tree is constructed from a first site by connecting it to $Z$ new sites, which constitute the first shell. One creates further shells by adding $Z-1$ new sites to every site in shell $s$. The Cayley tree has no loops, and all closed paths are self-retracing.[21] The Bethe lattice contains $s \to \infty$ shells. Since the Bethe lattice is bipartite, the chemical potential $\mu = U/2$ guarantees half-band filling at all temperatures.

We are interested in the local Green function of the Hubbard model in its exact ground state $|\Psi\rangle$. We use the abbreviation,

$$\langle\hat{A}\rangle = \frac{\langle\Psi|\hat{A}|\Psi\rangle}{\langle\Psi|\Psi\rangle} \tag{3}$$

for ground-state expectation values and define the local causal Green function in the time domain,

$$G_{\sigma}(i;t) = -\mathrm{i}\langle\hat{T}_{\mathrm{s}}\hat{c}_{i,\sigma}(t)\hat{c}^{\dagger}_{i,\sigma}(0)\rangle, \tag{4}$$

where the Heisenberg operators,

$$\hat{c}_{i,\sigma}(t) = e^{\mathrm{i}\hat{H}t}\hat{c}_{i,\sigma}e^{-\mathrm{i}\hat{H}t} \tag{5}$$

are time ordered with the help of the time-ordering operator $\hat{T}_{\mathrm{t}}$,

$$\hat{T}_{\mathrm{t}}\hat{c}_{i,\sigma}(t)\hat{c}^{\dagger}_{j,\sigma'}(t') = \begin{cases} \hat{c}_{i,\sigma}(t)\hat{c}^{\dagger}_{j,\sigma'}(t') & \text{for} \quad t > t', \\ -\hat{c}^{\dagger}_{j,\sigma'}(t')\hat{c}_{i,\sigma}(t) & \text{for} \quad t < t'. \end{cases} \tag{6}$$

The time-frequency Fourier transformation of the local Green function is defined as

$$G_{i,\sigma}(\omega) = \int_{-\infty}^{\infty} dt\, e^{\mathrm{i}\omega t} G_{\sigma}(i;t) \tag{7}$$

$$= \langle\hat{c}_{i,\sigma}(\omega - [\hat{H} - E_0(N)] + \mathrm{i}\eta)^{-1}\hat{c}^{\dagger}_{i,\sigma}\rangle + \langle\hat{c}^{\dagger}_{i,\sigma}(\omega + [\hat{H} - E_0(N)] - \mathrm{i}\eta)^{-1}\hat{c}_{i,\sigma}\rangle. \tag{8}$$

Henceforth, the limit $\eta \to 0^{+}$ is implicitly understood. In Eq. (8), $E_0(N)$ denotes the energy of the $N$-particle ground state $|\Psi\rangle$ of the Hubbard model. The (local) density of states is obtained from the imaginary part of the Green function [$\mathrm{sgn}(x)$ is the sign function],

$$D_{\sigma}(\omega) = -\frac{1}{\pi}\,\mathrm{sgn}(\omega)\,\mathrm{Im}[G_{i,\sigma}(\omega)]. \tag{9}$$

The density of states is positive semidefinite, and its integral over all frequencies is unity.[22]

The Green function for noninteracting electrons on a Bethe lattice ($U = 0$) can be calculated in various ways.[23] In the limit $Z \to \infty$, it approaches the Hubbard semiellipse,

$$\rho(\omega) = \frac{4}{\pi W}\sqrt{1 - \left(\frac{2\omega}{W}\right)^2} \quad \text{for} \quad |\omega| \leqslant W/2, \tag{10}$$

with $W = 4$ as the bare bandwidth. In the presence of interactions ($U > 0$), the local Green function can be expressed with the help of the (proper) self-energy $\Sigma_{\sigma}(\omega)$,

$$G_{i,\sigma}(\omega) = \int_{-\infty}^{\infty} d\omega' \frac{\rho(\omega')}{\omega - \omega' - \Sigma_{\sigma}(\omega)} = G^{(0)}_{i,\sigma}[\omega - \Sigma_{\sigma}(\omega)]. \tag{11}$$

Note that, in the limit $Z \to \infty$, the self-energy depends only on frequency.[2] In principle, the self-energy can be calculated in diagrammatic perturbation theory.[22]

#### 2. SIAM

In order to set up the DMFT for the half-filled paramagnetic Hubbard model, we consider the discrete symmetric SIAM in star geometry,

$$\hat{H}_{\mathrm{SIAM}} = \sum_{m=0}^{L-2}\sum_{\sigma}\xi_m\hat{a}^{\dagger}_{m,\sigma}\hat{a}_{m,\sigma} - \frac{U}{2}\sum_{\sigma}\hat{n}_{d,\sigma} + U\hat{n}_{d,\uparrow}\hat{n}_{d,\downarrow} + \sum_{m=0}^{L-2}\sum_{\sigma}V_m(\hat{a}^{\dagger}_{m,\sigma}\hat{d}_{\sigma} + \hat{d}^{\dagger}_{\sigma}\hat{a}_{m,\sigma}). \tag{12}$$

Here, $\hat{a}^{\dagger}_{m,\sigma}$ ($\hat{a}_{m,\sigma}$) creates (annihilates) a bath electron with spin $\sigma$ and bath energy $\xi_m$, $\hat{d}^{\dagger}_{\sigma}\hat{d}_{\sigma}$) creates (annihilates) an electron with spin $\sigma$ on the impurity level with energy $E_d = -U/2$, and $\hat{n}_{d,\sigma} = \hat{d}^{\dagger}_{\sigma}\hat{d}_{\sigma}$ counts the number of $\sigma$ electrons on the impurity. The Hubbard interaction on the impurity is the same as in the Hubbard model. The parameters $V_m > 0$ describe the hybridization between the bath levels and the impurity site. The half-filled case corresponds to $N = L$

electrons. Henceforth, the limits $N, L \to \infty$ are implicitly understood.

The SIAM is fully characterized by the hybridization function,[24]

$$\Delta(\omega) = \sum_m \frac{V_m^2}{\omega - \xi_m + \mathrm{i}\,\mathrm{sgn}(\omega)\eta}. \tag{13}$$

The (causal) Green function of the impurity electrons is defined by

$$G_\sigma^{\mathrm{SIAM}}(d;t) = -\mathrm{i}\langle \hat{T}_s \hat{d}_\sigma(t)\hat{d}_\sigma^\dagger(0)\rangle, \tag{14}$$

where the expectation value is to be taken in the exact ground state of the SIAM. After Fourier transformation, the Green function can be expressed with the help of the hybridization function and the (proper) self-energy in the form[24]

$$\begin{aligned} G_\sigma^{\mathrm{SIAM}}(\omega) &= \int_{-\infty}^{\infty} dt\, e^{\mathrm{i}\omega t} G_\sigma^{\mathrm{SIAM}}(d;t) \\ &= \frac{1}{\omega - \Delta(\omega) - \Sigma_\sigma^{\mathrm{SIAM}}(\omega)}. \end{aligned} \tag{15}$$

As in the case of the Hubbard model, the self-energy of the single-impurity model can be calculated in diagrammatic perturbation theory.

#### 3. DMFT equations on a Bethe lattice

The skeleton diagrams for the SIAM and the Hubbard model with an infinite coordination number are identical; for a review, see Ref. 1. Therefore, if their local Green functions agree,

$$G_{i,\sigma}(\omega) = G_\sigma^{\mathrm{SIAM}}(\omega), \tag{16}$$

their self-energies agree as well,

$$\Sigma_\sigma(\omega) = \Sigma_\sigma^{\mathrm{SIAM}}(\omega). \tag{17}$$

The exact solution of the Hubbard model for an infinite coordination number reduces to the calculation of the Green function of the SIAM for a general hybridization function $\Delta(\omega)$. The DMFT self-consistency equations (16) and (17) single out the hybridization function, which describes the Hubbard model in the limit of an infinite coordination number.

For the Hubbard model on a Bethe lattice, the semielliptic bare density of states (10) results in the following form of the local Green function (11):

$$G_{i,\sigma}(z) = \tfrac{1}{2}(z - \sqrt{z^2 - 4}), \quad z = \omega - \Sigma_\sigma(\omega), \tag{18}$$

so that

$$\Sigma_\sigma(\omega) = \omega - G_{i,\sigma}(\omega) - \frac{1}{G_{i,\sigma}(\omega)} \tag{19}$$

holds. Together with Eq. (15), the DMFT equations (16) and (17) reduce to the single condition

$$\Delta(\omega) = G_\sigma^{\mathrm{SIAM}}(\omega), \tag{20}$$

on the hybridization function. The remaining task is to calculate the Green function $G_\sigma^{\mathrm{SIAM}}(\omega)$ for the SIAM for a general hybridization function $\Delta(\omega)$. Equation (20) singles out the hybridization function, which describes the Hubbard model on a Bethe lattice with an infinite coordination number. From now on, we will exclusively investigate the SIAM Therefore, we drop the superscript SIAM on all quantities.

### B. Two-chain mapping for the Mott-Hubbard insulator

#### 1. Hubbard bands and charge gap

We are interested in the description of the Mott-Hubbard insulator where the charge gap separates the upper Hubbard band (UHB) and the LHB. Due to particle-hole and spin symmetry (see, for example, Refs. 6 and 25), it is sufficient to calculate the Green function of the LHB for a fixed spin, say, $\sigma = \uparrow$,

$$G_{\mathrm{LHB}}(\omega < 0) = \langle \hat{d}_\uparrow^\dagger (\omega + \hat{H} - E_0 - \mathrm{i}\eta)^{-1} \hat{d}_\uparrow \rangle. \tag{21}$$

For positive frequencies, $\omega > 0$, we have $G_{\mathrm{UHB}}(\omega) = -G_{\mathrm{LHB}}(-\omega)$. Moreover, for the density of states, we have $D_{\mathrm{UHB}}(\omega) = D_{\mathrm{LHB}}(-\omega)$, i.e., the density of states is symmetric around $\omega = 0$.

The upper edge of the LHB is the chemical potential $\mu^- < 0$ for adding the $L$th electron. The minimal energy for adding another electron to the system ($N = L + 1$), the chemical potential $\mu^+$, is given by $\mu^+ = -\mu^-$.[26] Therefore, the charge gap obeys

$$\Delta_{\mathrm{c}} = \mu^+ - \mu^- = 2|\mu^-|, \tag{22}$$

i.e., it can be obtained from the upper band edge of the LHB.

#### 2. Two-chain SIAM

The self-consistency equation (20) demands that the imaginary part of the hybridization function is identical to the density of states. For the Hubbard model at strong coupling, $U \gg W$, we know that the density of states is centered in the two Hubbard bands, $|\omega \pm U/2| \leqslant O(W/2)$.[27] For discrete bath levels, the imaginary part of the hybridization function $\Delta(\omega)$ in Eq. (13) consists of peaks at the bath energies $\xi_m$ with weights $V_m^2$. Therefore, the bath energies can be grouped into those of the LHB, $\xi_m = -O(U/2)$, and those of the UHB, $\xi_m = O(U/2)$. Consequently, we map the SIAM in star geometry, Eq. (12), onto a two-chain geometry where the impurity site hybridizes with two sites, which represent the LHB and the UHB.[28] Note that, in numerical treatments of the SIAM, the star geometry is usually mapped onto a single chain.[1] Apparently, the two-chain mapping is more adequate for the Mott-Hubbard insulator; a similar idea was proposed earlier in Refs. 5 and 29. The concept is readily generalized as a multichain mapping where each region with a finite density of states is represented by its own chain; see the following.

The two-chain mapping can be carried out technically along the lines of the single-chain mapping (Lanczos tridiagonalization[3]). The transformed Hamiltonian reads

$$\hat{H} = \hat{H}_0 + \hat{V} = \hat{H}_0 + \hat{V}_0 + \hat{V}_1 + \hat{V}_2, \tag{23}$$

$$\begin{aligned} \hat{H}_0 = &-\frac{U}{2} \sum_{l=0}^{(L-3)/2} \sum_\sigma (\hat{\alpha}_{l,\sigma}^\dagger \hat{\alpha}_{l,\sigma} - \hat{\beta}_{l,\sigma}^\dagger \hat{\beta}_{l,\sigma}) \\ &+ U(\hat{n}_{d,\uparrow} - 1/2)(\hat{n}_{d,\downarrow} - 1/2), \end{aligned} \tag{24}$$

$$\hat{V}_0 = \sqrt{\frac{1}{2}} \sum_{\sigma} [(\hat{d}^{\dagger}_{\sigma} \hat{\alpha}_{0,\sigma} + \hat{d}^{\dagger}_{\sigma} \hat{\beta}_{0,\sigma}) + \text{H.c.}],$$

$$\hat{V}_1 = \sum_{l=0}^{(L-3)/2} \sum_{\sigma} t_l [(\hat{\alpha}^{\dagger}_{l,\sigma} \hat{\alpha}_{l+1,\sigma} + \hat{\beta}^{\dagger}_{l,\sigma} \hat{\beta}_{l+1,\sigma}) + \text{H.c.}], \quad (25)$$

$$\hat{V}_2 = \sum_{l=0}^{(L-3)/2} \sum_{\sigma} \varepsilon_l (\hat{\alpha}^{\dagger}_{l,\sigma} \hat{\alpha}_{l,\sigma} - \hat{\beta}^{\dagger}_{l,\sigma} \hat{\beta}_{l,\sigma}).$$

The $\hat{\alpha}$ operators describe the electrons in the lower chain (LHB), and the $\hat{\beta}$ operators describe those in the upper chain (UHB). Due to particle-hole symmetry, the electron-transfer amplitudes in the lower and upper chains are equal, $t_l^- = t_l^+$, and the on-site energies in the lower and upper chains are opposite in sign, $\varepsilon_l^- = -\varepsilon_l^+ = \varepsilon_l - U/2$. The mapping is shown in Fig. 1. Later, we will investigate the model in the strong-coupling limit. Therefore, we separated the Hamiltonian into the starting Hamiltonian $\hat{H}_0$, Eq. (24), and the perturbation $\hat{V}$, Eq. (25). Note that $\hat{H}_0$ describes the atomic limit $\hat{T} \equiv 0$, where there is no transfer between sites in the Hubbard model.

Our task is the calculation of the Green function on the impurity site, Eq. (21), for general on-site energies $\varepsilon_l$ and electron-transfer parameters $t_l$. In the two-chain geometry, these parameters assume the role of the energies $\xi_m$ and the hybridizations $V_m$ in the star geometry. Our approach relies on the order-by-order expansion of all quantities in $1/U$,

$$\varepsilon_l = \sum_{n=0}^{\infty} \varepsilon_l^{(n)} \left(\frac{1}{U}\right)^n, \quad t_l = \sum_{n=0}^{\infty} t_l^{(n)} \left(\frac{1}{U}\right)^n \quad (26)$$

for $l \geqslant 0$, whereby we implement the self-consistency equation (20).

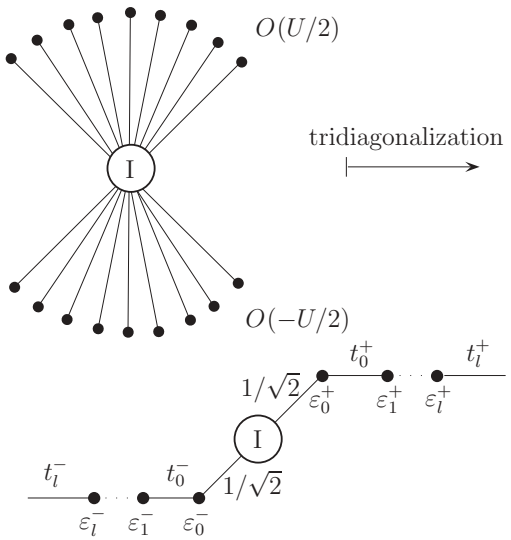


FIG. 1. Mapping of the discretized SIAM onto two semi-infinite chains, coupled via the impurity. The states, which have the energy $\xi_m = (U/2)$ and $\xi_m = -(U/2)$ in the atomic limit are mapped onto the upper and lower chains, respectively.

## III. SELF-CONSISTENCY EQUATION

### A. Results from Kato-Takahashi perturbation theory

In order to calculate the zero-temperature Green function for the SIAM in strong coupling, we adapt the Kato-Takahashi perturbation theory.[18,19] The Kato-Takahashi perturbation theory is particularly suitable for Hamiltonians $\hat{H} = \hat{H}_0 + \hat{V}$ where the ground state of the unperturbed Hamiltonian $\hat{H}_0$ is degenerate. Details can be found in Ref. 20.

The Green function of the LHB (21) can be transformed into

$$G_{\text{LHB}}(\omega) = \sum_{i=0}^{\infty} \langle \Phi | \tilde{d}^{\dagger}_{i,\uparrow} \big[ (\omega + U/2 + iU) \hat{\Gamma}^{(0)}_{i,L-1} + \hat{\mathcal{L}}_{i,L-1} - i\eta \big]^{-1} \tilde{d}_{i,\uparrow} | \Phi \rangle. \quad (27)$$

Here, the index $i$ labels the order of the Hubbard sub-bands, where $i = 0$ corresponds to the primary Hubbard sub-band. We will drop the index $i = 0$ whenever possible. We defined the state,

$$|\Phi\rangle := \frac{1}{\sqrt{2}} (|\phi_{\uparrow}\rangle + |\phi_{\downarrow}\rangle), \quad (28)$$

which is a symmetric mixture of the two ground states of the single-impurity model in the atomic limit at half band-filling,

$$|\phi_{\uparrow}\rangle = \hat{d}^{\dagger}_{\uparrow} \prod_{l=0}^{(L-3)/2} \hat{\alpha}^{\dagger}_{l,\uparrow} \hat{\alpha}^{\dagger}_{l,\downarrow} |\text{vac}\rangle, \quad (29)$$

$$|\phi_{\downarrow}\rangle = \hat{d}^{\dagger}_{\downarrow} \prod_{l=0}^{(L-3)/2} \hat{\alpha}^{\dagger}_{l,\uparrow} \hat{\alpha}^{\dagger}_{l,\downarrow} |\text{vac}\rangle. \quad (30)$$

Moreover, we need the reduced operators,

$$\tilde{d}_{i,\sigma} = \hat{\Gamma}^{\dagger}_{i,L-1} \hat{d}_{\sigma} \hat{\Gamma}_{0,L}, \quad \tilde{d}^{\dagger}_{i,\sigma} = (\tilde{d}_{i,\sigma})^{\dagger}, \quad (31)$$

$$\tilde{h}_{i,L-1} = \hat{\Gamma}^{\dagger}_{i,L-1} \hat{H} \hat{\Gamma}_{i,L-1}. \quad (32)$$

The reduced Hamilton operator $\tilde{h}_{i,L-1}$ describes the dynamics of a hole in the symmetric Anderson model. The operators $\hat{\Gamma}_{i,N}$ are the Kato-Takahashi projection operators.[6,18–20] The reduced Hamilton operators enter Eq. (27) in the combination,

$$\hat{\mathcal{L}}_{i,L-1} = \tilde{h}_{i,L-1} - (E_{0,L} + U/2 + iU) \hat{\Gamma}^{(0)}_{i,L-1}, \quad (33)$$

where $E_{0,L}$ is the ground-state energy of the symmetric Anderson model.

### B. Matrix representation of the self-consistency equation

The self-consistency equation (20) must be solved for all frequencies in the respective sub-bands of the LHB. The density of states of the individual sub-bands can be viewed as probability distributions, which can be characterized by their moments. The idea is to express the Green function and the hybridization function by their moments so that the self-consistency equation reduces to the condition that the two sets of moments agree. In this way, only a countable set of numbers must be compared. A suitable way to generate moments from a Green function is provided by the Lanczos iteration procedure.

#### 1. Lanczos iteration

For the starting vector $|0\rangle$ and the Hermitian operator $\hat{O}$, we use the following form of the Lanczos iteration:

$$\begin{aligned} |1\rangle &= -\hat{O}|0\rangle + a_0|0\rangle, \\ |n+1\rangle &= -\hat{O}|n\rangle + a_n|n\rangle + b_{n-1}|n-1\rangle, \quad n \geqslant 1, \end{aligned} \tag{34}$$

where

$$a_n = \frac{\langle n|\hat{O}|n\rangle}{\langle n|n\rangle}, \quad n \geqslant 0, \tag{35}$$

$$b_{n-1} = \frac{\langle n-1|\hat{O}|n\rangle}{\langle n-1|n-1\rangle} = -\frac{\langle n|n\rangle}{\langle n-1|n-1\rangle}, \quad n \geqslant 1. \tag{36}$$

The matrix representation $\mathfrak{O}$ of $\hat{O}$ within the Lanczos basis $\{|n\rangle\}$ is tridiagonal and symmetric, and we have

$$\mathfrak{O}_{n,n} = \frac{\langle n|\hat{O}|n\rangle}{\langle n|n\rangle} = a_n, \tag{37}$$

$$\mathfrak{O}_{n-1,n} = \frac{\langle n-1|\hat{O}|n\rangle}{\sqrt{\langle n-1|n-1\rangle}\sqrt{\langle n|n\rangle}} = -\sqrt{-b_n}. \tag{38}$$

In the following, we use Fraktur letters for the matrix representations of the corresponding operators in their Lanczos basis.

#### 2. Hybridization function

We introduce electron baths for every sub-band of the LHB. Starting from the SIAM in star geometry, we write the hybridization function in the form $\Delta_{\mathrm{LHB}}(\omega) = \sum_{i=0}^{\infty} \Delta_i(\omega)$,

$$\Delta_i(\omega) = \sum_m \frac{V_{i,m}^2}{(\omega + U/2 + iU) - \xi_{i;m} - \mathrm{i}\eta}, \tag{39}$$

where $\Delta_i(\omega)$ denotes the contribution of the $i$th sub-band. We cast each $\Delta_i(\omega)$ into matrix form by applying the Lanczos iteration with the starting vector,

$$|0\rangle_i := \frac{1}{\sqrt{g_i}} \sum_m V_{i,m} \hat{a}^\dagger_{i;m,\sigma}|\mathrm{vac}\rangle, \tag{40}$$

where $g_i$ is the weight of the $i$th sub-band in the density of states, $\sum_i g_i = 1/2$. With the (discretized) Hamiltonian for the bath electrons in star geometry,

$$\hat{H}_{\Delta,i} = \sum_{m,\sigma} \xi_{i,m} \hat{a}^\dagger_{i;m,\sigma} \hat{a}_{i;m,\sigma}, \tag{41}$$

we may write

$$\begin{aligned} \Delta_i(\omega) &= {}_i\langle 0|[(\omega + U/2 + iU) - \hat{H}_{\Delta,i} - \mathrm{i}\eta]^{-1}\,|0\rangle_i \\ &\equiv \{[(\omega + U/2 + iU)1 - \mathfrak{h}_{\Delta,i} - \mathrm{i}\eta]^{-1}\}_{00}. \end{aligned} \tag{42}$$

This form can be verified by noting that $[\hat{H}_{\Delta,i}]^n|0\rangle_i = 1/\sqrt{g_i}\sum_{m,\sigma} V_{i,m}(\xi_{i,m})^n \hat{a}^\dagger_{i;m,\sigma}|\mathrm{vac}\rangle$.

We note that the mapping of the single-impurity model from the star geometry to the multichain geometry is based on the Lanczos procedure.[3] Therefore, the starting vector $|0\rangle_i$ is identical to an electron at the first site, $|0\rangle_i = (1/\sqrt{2})\hat{\alpha}^\dagger_{i;0,\sigma}|\mathrm{vac}\rangle$, of the $i$th lower chain in the multichain geometry. Thus, the Hamiltonian $\hat{H}_{\Delta,i}$ for the bath electrons can also be written in the form

$$\hat{H}_{\Delta,i} := \sum_{l;\sigma} t_{i;l}(\hat{\alpha}^\dagger_{i;l,\sigma}\hat{\alpha}_{i;l+1,\sigma} + \mathrm{H.c.}) + \varepsilon_{i;l}\hat{\alpha}^\dagger_{i;l,\sigma}\hat{\alpha}_{i;l,\sigma}. \tag{43}$$

Then, the matrix $\mathfrak{h}_{\Delta,i}$ representing $\hat{H}_{\Delta,i}$ in the Lanczos basis reads

$$\mathfrak{h}_{\Delta,i} = \begin{pmatrix} \varepsilon_{i;0} & t_{i;0} & & & \\ t_{i;0} & \varepsilon_{i;1} & t_{i;1} & & \\ & t_{i;1} & \varepsilon_{i;2} & t_{i;2} & \\ & & \ddots & \ddots & \ddots \end{pmatrix}, \tag{44}$$

where the entries not shown are zero. The parameters $\varepsilon_{i;m}$ and $t_{i;m}$ define the SIAM in its multichain geometry.

#### 3. Green function

For the Green function (27), we use

$$|\Psi_0\rangle = \tilde{d}_\uparrow|\Phi\rangle, \tag{45}$$

as the starting vector, see Eq. (28), and

$$\hat{O} = \hat{\mathcal{L}}_{i,L-1}, \tag{46}$$

as the operator in the Lanczos iteration. In this way, we obtain the matrix representation,

$$G_{\mathrm{LHB}}(\omega) = \sum_{i=0}^{\infty} \{[(\omega + U/2 + iU)\mathbb{1} + \mathfrak{L}_i - \mathrm{i}\eta]^{-1}\}_{00}, \tag{47}$$

where the structure of $\mathfrak{L}_i$ is given by

$$\mathfrak{L}_i = \begin{pmatrix} e_{i;0} & \tau_{i;0} & & & \\ \tau_{i;0} & e_{i;1} & \tau_{i;1} & & \\ & \tau_{i;1} & e_{i;2} & \tau_{i;2} & \\ & & \ddots & \ddots & \ddots \end{pmatrix}. \tag{48}$$

The parameters $e_{i;m}$ and $\tau_{i;m}$ must be calculated from Eqs. (37) and (38).

#### 4. Self-consistency equation

For $t \equiv 1$ as our unit of energy, the self-consistency equation (20) reads ($\omega < 0$)

$$\begin{aligned} &\sum_{i=0}^{\infty} \{[(\omega + U/2 + iU)\mathbb{1} - \mathfrak{h}_{\Delta,i} - \mathrm{i}\eta]^{-1}\}_{00} \\ &\quad = \sum_{i=0}^{\infty} \{[(\omega + U/2 + iU)\mathbb{1} + \mathfrak{L}_i - \mathrm{i}\eta]^{-1}\}_{00}. \end{aligned} \tag{49}$$

In this paper, we are mainly interested in the primary LHB. As shown in Ref. 20, it is the only LHB with nonvanishing spectral weight up to and including third order in $1/U$. Therefore, up to this order, we may write

$$\begin{aligned} &\{[(\omega + U/2)1 - \mathfrak{h}_\Delta - \mathrm{i}\eta]^{-1}\}_{00} \\ &\quad = \{[(\omega + U/2)\mathbb{1} + \mathfrak{L} - \mathrm{i}\eta]^{-1}\}_{00}, \end{aligned} \tag{50}$$

where we have dropped the subscript $i = 0$. Reckoning with Eq. (50), we realize that

$$\mathfrak{h}_\Delta = -\mathfrak{L} \tag{51}$$

is a sufficient condition to ensure the self-consistency. From the continued fraction expansion of the hybridization function

and the Green function, it can readily be shown that it also is a necessary condition. Therefore, the self-consistency condition reduces to

$$\varepsilon_n = -e_n \quad \text{and} \quad |t_n| = |\tau_n|. \tag{52}$$

Note that Eq. (52) is a vast simplification over Eq. (20) because, due to the matrix structure, we only have to equate numbers and not functions. However, since all our calculations are implicitly performed in the thermodynamic limit, there is a (countably) infinite set of parameters to fix. As we will show explicitly up to third order in $1/U$, the locality of the Hubbard interaction guarantees that there is an index $l_m$ in $m$th-order perturbation theory such that the Lanczos parameters $\tau_n$ and $e_n$ become constant for $n \geqslant l_m$.

## IV. SOLUTION OF THE DMFT EQUATION

In Sec. IV A, we show how the DMFT equation is solved for leading order in $1/U$. In Sec. IV B, we summarize the results for third order.

### A. Calculations for leading order

First, we calculate the ground-state energy and set up the starting vector for the Lanczos iteration. Next, we calculate the action of the Lanczos operator on the states with a single hole in the lower Hubbard chain. Then, we derive the parameters $\varepsilon_0^{(0)}$, $\varepsilon_1^{(0)}$, $t_0^{(0)}$, and $t_1^{(0)}$ from the first two Lanczos iterations. Lastly, we prove the results $\varepsilon_l^{(0)} = 0$ and $t_l^{(0)} = 1$ for all $l$ by induction.

#### 1. Ground-state energy and starting vector for the Lanczos iteration

For leading order, the ground state at half band-filling is not transformed to leading order $|\Psi^{(0)}\rangle = |\Phi\rangle$. The correction to the ground-state energy for leading order reads

$$E_{0,L}^{[0]} = \langle\phi_\uparrow|\hat{V}|\phi_\uparrow\rangle = \langle\phi_\uparrow|\hat{V}_2|\phi_\uparrow\rangle = 2\sum_{l=0}^{(L-3)/2}\varepsilon_l. \tag{53}$$

The operators $\hat{V}_0$ and $\hat{V}_1$ do not contribute because they modify $|\phi_\uparrow\rangle$. The contribution of $\hat{V}_2$ is readily calculated because the sites of the lower chain are doubly occupied, see Eq. (25).

According to Eq. (45), the starting vector for the Lanczos iteration is given by

$$\begin{aligned} \left|\Psi_0^{(0)}\right\rangle &= \hat{\Gamma}_{L-1}^{(0)}\hat{d}_\uparrow\hat{\Gamma}_L^{(0)}|\Phi\rangle \equiv |\phi_{-1}\rangle, \\ |\phi_{-1}\rangle &= \sqrt{\frac{1}{2}}\hat{d}_\uparrow|\phi_\uparrow\rangle = \sqrt{\frac{1}{2}}\prod_{l=0}^{(L-3)/2}\hat{\alpha}_{l,\uparrow}^\dagger\hat{\alpha}_{l,\downarrow}^\dagger|\text{vac}\rangle. \end{aligned} \tag{54}$$

Note that, in general, the starting vector is not normalized for unity.

#### 2. Lanczos operator

The operator for the Lanczos iteration (46) is given by

$$\hat{\mathcal{L}}_{L-1}^{(0)} = \hat{\Gamma}_{L-1}^{(0)}\left(\hat{V} - E_{0,L}^{[0]}\right)\hat{\Gamma}_{L-1}^{(0)}. \tag{55}$$

In the course of the calculations, we will need the eigenbasis of $\hat{\Gamma}_{L-1}^{(0)}$, i.e., single-hole states in the half-filled ground states of $\hat{H}_0$. Apart from $|\phi_{-1}\rangle$ in Eq. (54), we define, for $n \geqslant 0$ [see Eqs. (29) and (30)],

$$\begin{aligned} |\phi_{n;u}\rangle &:= \sqrt{\frac{1}{2}}\hat{d}_\downarrow^\dagger\hat{\alpha}_{n,\downarrow}\prod_{l=0}^{(L-3)/2}\hat{\alpha}_{l,\uparrow}^\dagger\hat{\alpha}_{l,\downarrow}^\dagger|\text{vac}\rangle, \\ |\phi_{n;d}\rangle &:= -\sqrt{\frac{1}{2}}\hat{d}_\uparrow^\dagger\hat{\alpha}_{n,\uparrow}\prod_{l=0}^{(L-3)/2}\hat{\alpha}_{l,\uparrow}^\dagger\hat{\alpha}_{l,\downarrow}^\dagger|\text{vac}\rangle, \\ |\chi_n\rangle &:= -\sqrt{\frac{1}{2}}\hat{d}_\downarrow^\dagger\hat{\alpha}_{n,\uparrow}\prod_{l=0}^{(L-3)/2}\hat{\alpha}_{l,\uparrow}^\dagger\hat{\alpha}_{l,\downarrow}^\dagger|\text{vac}\rangle, \end{aligned} \tag{56}$$

and their useful linear combinations,

$$\begin{aligned} |\gamma_n\rangle &:= (-1)^n\sqrt{\frac{1}{2}}(|\phi_{n;u}\rangle - |\phi_{n;d}\rangle), \\ |m_{n;u}\rangle &:= (-1)^n\sqrt{\frac{1}{2}}(|\phi_{n;u}\rangle + |\chi_n\rangle), \\ |m_{n;d}\rangle &:= (-1)^n\sqrt{\frac{1}{2}}(|\phi_{n;d}\rangle + |\chi_n\rangle). \end{aligned} \tag{57}$$

Note that the states are not normalized, but they are site orthogonal in the sense that the overlap between states with different site indices is zero.

The action of the Lanczos operator $\hat{\mathcal{L}}_{L-1}^{(0)}$ on the states is readily calculated. One finds for $n = 0$,

$$\begin{aligned} \hat{\mathcal{L}}_{L-1}^{(0)}|\phi_{-1}\rangle &= |\gamma_0\rangle, \\ \hat{\mathcal{L}}_{L-1}^{(0)}|\gamma_0\rangle &= |\phi_{-1}\rangle - \varepsilon_0^{(0)}|\gamma_0\rangle + t_0^{(0)}|\gamma_1\rangle, \\ \hat{\mathcal{L}}_{L-1}^{(0)}|m_{0;u}\rangle &= \tfrac{1}{2}|\phi_{-1}\rangle - \varepsilon_0^{(0)}|m_{0;u}\rangle + t_0^{(0)}|m_{1;u}\rangle, \\ \hat{\mathcal{L}}_{L-1}^{(0)}|m_{0;d}\rangle &= -\tfrac{1}{2}|\phi_{-1}\rangle - \varepsilon_0^{(0)}|m_{0;d}\rangle + t_0^{(0)}|m_{1;d}\rangle, \end{aligned} \tag{58}$$

and, for $n \geqslant 1$ and $x_n = \gamma_n, m_{n;u}, m_{n;d}$,

$$\hat{\mathcal{L}}_{L-1}^{(0)}|x_n\rangle = t_{n-1}^{(0)}|x_{n-1}\rangle - \varepsilon_n^{(0)}|x_n\rangle + t_n^{(0)}|x_{n+1}\rangle. \tag{59}$$

The application of the Lanczos operator results in the same structure for all $n \geqslant 1$. Note that this holds true in $m$th-order perturbation theory in $1/U$ for $n \geqslant m + 1$.

#### 3. First and second Lanczos iterations

In the first Lanczos iteration, we must determine the state,

$$\left|\Psi_1^{(0)}\right\rangle := -\hat{\mathcal{L}}_{L-1}^{(0)}\left|\Psi_0^{(0)}\right\rangle + e_0^{(0)}\left|\Psi_0^{(0)}\right\rangle, \tag{60}$$

with

$$e_0^{(0)} = \frac{\left\langle\Psi_0^{(0)}\right|\hat{\mathcal{L}}_{L-1}^{(0)}\left|\Psi_0^{(0)}\right\rangle}{\left\langle\Psi_0^{(0)}\middle|\Psi_0^{(0)}\right\rangle}. \tag{61}$$

With the help of Eq. (58), we find

$$\left|\Psi_1^{(0)}\right\rangle = -|\gamma_0\rangle, \quad e_0^{(0)} = 0, \tag{62}$$

because $e_0^{(0)} = 2\langle\phi_{-1}|\gamma_0\rangle = 0$. The self-consistency equation (52) then gives $\varepsilon_0^{(0)} = 0$. Furthermore, we have

$$\tau_0^{(0)} = \frac{\left\langle\Psi_0^{(0)}\right|\hat{\mathcal{L}}_{L-1}^{(0)}\left|\Psi_1^{(0)}\right\rangle}{\left\langle\Psi_0^{(0)}\middle|\Psi_0^{(0)}\right\rangle} = -2\langle\gamma_0|\gamma_0\rangle = -1, \tag{63}$$

so that $t_0^{(0)} = 1$ follows from the self-consistency equation (52).

In the second iteration, we can use the results from the first iteration. We calculate

$$\left|\Psi_2^{(0)}\right\rangle := -\hat{\mathcal{L}}_{L-1}^{(0)}\left|\Psi_1^{(0)}\right\rangle + e_1^{(0)}\left|\Psi_1^{(0)}\right\rangle + \tau_0^{(0)}\left|\Psi_0^{(0)}\right\rangle, \tag{64}$$

with

$$e_1^{(0)} = \frac{\left\langle\Psi_1^{(0)}\right|\hat{\mathcal{L}}_{L-1}^{(0)}\left|\Psi_1^{(0)}\right\rangle}{\left\langle\Psi_1^{(0)}\middle|\Psi_1^{(0)}\right\rangle} = 2(\langle\gamma_0|\phi_{-1}\rangle + \langle\gamma_0|\gamma_1\rangle) = 0, \tag{65}$$

where we used $\varepsilon_0^{(0)} = 0$ and $t_0^{(0)} = 1$ in Eq. (58). The self-consistency equation (52) then gives $\varepsilon_1^{(0)} = 0$.

The second state in the Lanczos iteration reduces to

$$\left|\Psi_2^{(0)}\right\rangle = |\gamma_1\rangle, \tag{66}$$

and we find

$$\tau_1^{(0)} = -2\left(\langle\phi_{-1}|\gamma_1\rangle + \langle\gamma_1|\gamma_1\rangle\right) = -1, \tag{67}$$

so that $t_1^{(0)} = 1$ follows from the self-consistency equation (52).

#### 4. Induction

Now, we are in the position to prove, by induction, that $\varepsilon_n^{(0)} = e_n^{(0)} = 0$ and $\tau_n^{(0)} = -1 = -t_n^{(0)}$. Let this assumption be true for $1 \leqslant n \leqslant M-2$ $(M \geqslant 3)$ and assume, for $1 \leqslant n \leqslant M-1$ $(M \geqslant 3)$, that

$$\left|\Psi_n^{(0)}\right\rangle = (-1)^n|\gamma_{n-1}\rangle. \tag{68}$$

Then, we calculate

$$\left|\Psi_M^{(0)}\right\rangle := -\hat{\mathcal{L}}_{L-1}^{(0)}\left|\Psi_{M-1}^{(0)}\right\rangle + e_{M-1}^{(0)}\left|\Psi_{M-1}^{(0)}\right\rangle + \tau_{M-2}^{(0)}\left|\Psi_{M-2}^{(0)}\right\rangle, \tag{69}$$

with

$$\begin{aligned} e_{M-1}^{(0)} &= \frac{\left\langle\Psi_{M-1}^{(0)}\right|\hat{\mathcal{L}}_{L-1}^{(0)}\left|\Psi_{M-1}^{(0)}\right\rangle}{\left\langle\Psi_{M-1}^{(0)}\middle|\Psi_{M-1}^{(0)}\right\rangle} \\ &= -2(\langle\gamma_{M-2}|\gamma_{M-3}\rangle + \langle\gamma_{M-2}|\gamma_{M-1}\rangle) = 0, \end{aligned} \tag{70}$$

where we used $\varepsilon_{M-2}^{(0)} = 0$ and $t_{M-2}^{(0)} = t_{M-3}^{(0)} = 1$ in Eq. (59). The self-consistency equation (52) then gives $\varepsilon_{M-1}^{(0)} = 0$, which proves the next step in the induction for $\varepsilon_n^{(0)}$.

The next state in the Lanczos iteration reduces to

$$\begin{aligned} \left|\Psi_M^{(0)}\right\rangle &= (-1)^M(|\gamma_{M-3}\rangle + |\gamma_{M-1}\rangle) - (-1)^{M-2}|\gamma_{M-3}\rangle \\ &= (-1)^M|\gamma_{M-1}\rangle, \end{aligned} \tag{71}$$

which proves the next step in the induction for $|\Psi_n^{(0)}\rangle$.

Finally, we find

$$\begin{aligned} \tau_{M-1}^{(0)} &= \frac{\left\langle\Psi_{M-1}^{(0)}\right|\hat{\mathcal{L}}_{L-1}^{(0)}\left|\Psi^{(0)}\right\rangle}{\left\langle\Psi_{M-1}^{(0)}\middle|\Psi_{M-1}^{(0)}\right\rangle} \\ &= -2(\langle\gamma_{M-3}|\gamma_{M-1}\rangle + \langle\gamma_{M-1}|\gamma_{M-1}\rangle) = -1, \end{aligned} \tag{72}$$

so that $t_{M-1}^{(0)} = 1$ follows from the self-consistency equation (52). This proves the next step in the induction for $t_n^{(0)}$.

We recall that our approach strongly relies on the simple form of Eq. (20) of the self-consistency equation. For a general form of the bare density of states $\rho(\omega)$, the calculation of the density of states for the LHB for leading order is a demanding task.[30]

### B. Results up to third order

The calculations up to third order are straightforward but tedious. Simplifications arise from the fact that we are interested in the half-filled case $(N = L)$ and the situation with a single hole $(N = L-1)$. Moreover, the results for leading order simplify the analysis considerably. Details are given in Ref. 20.

Here, we summarize the results,

$$\begin{aligned} \varepsilon_0 &= \frac{7}{4U^3}, \quad \varepsilon_1 = \frac{1}{2U} + \frac{31}{8U^3}, \\ \varepsilon_n &= \frac{1}{2U} + \frac{35}{8U^3} \equiv \bar{\varepsilon} \quad (n \geqslant 2), \\ t_0 &= 1 + \frac{1}{8U^2}, \quad t_n = 1 + \frac{3}{8U^2} \equiv \bar{t} \quad (n \geqslant 1). \end{aligned} \tag{73}$$

Note that only odd (even) orders appear in the $1/U$ expansion of $\varepsilon_l$ $(t_l)$.

## V. HUBBARD BANDS IN THIRD ORDER

### A. Density of states of the LHB

The hybridization function $\Delta(\omega)$, or equivalently, the impurity Green function, can be obtained from an equivalent scattering problem for a single particle on a semi-infinite chain. We start this section by formulating this problem. Next, we calculate the single-particle gap and the hybridization function in closed form. Lastly, we expand this expression order by order in $1/U$, which defines the band-part Green function.

#### 1. Scattering problem

The Lanczos algorithm provides the tridiagonal matrix representation of the hybridization function,

$$\mathfrak{h}_\Delta = \begin{pmatrix} \varepsilon_0 & t_0 & & & \\ t_0 & \varepsilon_1 & \bar{t} & & \\ & \bar{t} & \bar{\varepsilon} & \bar{t} & \\ & & \ddots & \ddots & \ddots \end{pmatrix}, \tag{74}$$

where the parameters are given in Eq. (73).

As shown in Sec. III, the hybridization function can be obtained from

$$\Delta_{\mathrm{LHB}}(\omega) = w\{[(\omega + U/2)\mathbb{1} - \mathfrak{h}_\Delta - \mathrm{i}\eta]^{-1}\}_{00}. \tag{75}$$

The matrix $\mathfrak{h}_\Delta$ (74) corresponds to a tight-binding Hamiltonian $\hat{K}$, which describes the transfer of a single particle on a semi-infinite chain; compare Eq. (25), plus a scattering potential $\hat{W}$ at the boundary of the chain,

$$\begin{aligned} \hat{H}_{\mathrm{scat}} &= \hat{K} + \hat{W}, \\ \hat{K} &= \bar{t}\sum_{l=0}^{\infty}(|l\rangle\langle l+1| + |l+1\rangle\langle l|) + \bar{\varepsilon}\sum_{l=0}^{\infty}|l\rangle\langle l|, \\ \hat{W} &= \varepsilon_0^*|0\rangle\langle 0| + \varepsilon_1^*|1\rangle\langle 1| + t_0^*\left(|0\rangle\langle 1| + |1\rangle\langle 0|\right), \end{aligned} \tag{76}$$

with $\varepsilon_0^* = \varepsilon_0 - \bar{\varepsilon} = -1/(2U) - 21/(8U^3)$, $\varepsilon_1^* = \varepsilon_1 - \bar{\varepsilon} = -1/(2U^3)$, and $t_0^* = t_0 - \bar{t} = -1/(4U^2)$. Note that the scattering potential $\hat{W}$ is attractive, which results in a redshift of the density of states; see the following.

The hybridization function can equally be calculated from the one-particle Hamiltonian $\hat{H}_{\rm scat}$,

$$\begin{aligned}\Delta_{\rm LHB}(\omega) &= \{[(\omega+U/2)\mathbb{1}-\mathfrak{h}_\Delta-\mathrm{i}\eta]^{-1}\}_{00}\\ &= \tfrac{1}{2}\langle 0|[(\omega+U/2)\mathbb{1}-\hat{H}_{\rm scat}-\mathrm{i}\eta]^{-1}|0\rangle. \end{aligned}\quad (77)$$

In this way, the Green function for the LHB can be deduced from a one-particle problem.

### 2. Single-particle gap

The attractive $\hat{W}$ is too weak to generate a bound state below the lower band edge of the tight-binding operator $\hat{K}$. Therefore, it does not change the support of the imaginary part of the bare Green function defined by $\hat{K}$, which is given by $|\omega-\bar{\epsilon}|\leqslant 2\bar{t}$. In turn, this implies that the upper edge for the LHB is given by $\mu^- = -U/2+\bar{\epsilon}+2\bar{t}$ so that the charge gap in Eq. (22) is given by (bandwidth $W=4$),

$$\begin{aligned}\Delta_{\rm c} &= 2|-U/2+\bar{\epsilon}+2\bar{t}|\\ &= U-4-\frac{1}{U}-\frac{3}{2U^2}-\frac{35}{4U^3}+O\left(\frac{1}{U^4}\right).\end{aligned}\quad (78)$$

The result for second order was derived earlier by Eastwood *et al.*[6] Note that the coefficient for third order is larger than anticipated in Ref. 6.

Let $\Delta_{\rm c}(U_{\rm c})$ denote the critical value of the on-site interaction $U$ where the charge gap closes, i.e., $\Delta_{\rm c}(U_{\rm c})=0$. Up to third order, we find

$$\begin{aligned}U_{\rm c}^{(0)} &= 4, \quad U_{\rm c}^{(1)} = 4.236\ [5.90\%],\\ U_{\rm c}^{(2)} &= 4.313\ [1.82\%], \quad U_{\rm c}^{(3)} = 4.406\ [2.16\%],\end{aligned}\quad (79)$$

where the number in square brackets gives the percentage change to the result of the previous order. Apparently, the changes in the estimated critical interaction strength from the second to the third order are of the same order of magnitude, and the critical interaction strength does not converge quickly in these low orders.

### 3. Green function for the scattering problem

The calculation of the boundary Green function for a semi-infinite chain with a local potential at the boundary is readily accomplished.[31,32] We define the general two-site Green functions,

$$g_{l,m}(\omega) = \langle l|[(\omega+U/2)\mathbb{1}-\hat{H}_{\rm scat}-\mathrm{i}\eta]^{-1}|m\rangle, \quad (80)$$

$$g^{(0)}_{l,m}(\omega) = \langle l|[(\omega+U/2)\mathbb{1}-\hat{K}-\mathrm{i}\eta]^{-1}|m\rangle. \quad (81)$$

The Green functions (81) for the tight-binding Hamiltonian $\hat{K}$ are calculated explicitly in Ref. 20.

In Eq. (80), we use the operator identity $(\hat{A}-\hat{B})^{-1} = \hat{A}^{-1}+\hat{A}^{-1}\hat{B}(\hat{A}-\hat{B})^{-1}$ with $\hat{A} = (\omega+U/2)\mathbb{1}-\hat{K}$ and $\hat{B}=\hat{W}$ so that we can write

$$\begin{aligned}g_{0,0}(\omega) &= g^{(0)}_{0,0}(\omega)+\sum_{l,m=0}^{\infty} g^{(0)}_{0,l}(\omega)\langle l|\hat{W}|m\rangle g_{m,0}(\omega) \quad (82)\\ &= g^{(0)}_{0,0}(\omega)+\epsilon_0^* g^{(0)}_{0,0}(\omega)g_{0,0}(\omega)+\epsilon_1^* g^{(0)}_{0,1}(\omega)g_{1,0}(\omega)\\ &\quad +t_0^*\big[g^{(0)}_{0,0}(\omega)g_{1,0}(\omega)+g^{(0)}_{0,1}(\omega)g_{0,0}(\omega)\big],\end{aligned}$$

where we used the locality of the scattering potential $\hat{W}$ (76) in the second step. Likewise, we obtain

$$\begin{aligned}g_{1,0}(\omega) &= g^{(0)}_{1,0}(\omega)+\epsilon_0^* g^{(0)}_{1,0}(\omega)g_{0,0}(\omega)+\epsilon_1^* g^{(0)}_{1,1}(\omega)g_{1,0}(\omega)\\ &\quad +t_0^*\big[g^{(0)}_{1,1}(\omega)g_{0,0}(\omega)+g^{(0)}_{1,0}(\omega)g_{1,0}(\omega)\big].\end{aligned}\quad (83)$$

We can solve the coupled equations (82) and (83) to give our final result [$g_{0,0}(\omega)=2G_{\rm LHB}(\omega)$],

$$\begin{aligned}g_{0,0}(\omega) &= \frac{g^{(0)}_{0,0}(\omega)-\varepsilon_1^*\big[g^{(0)}_{0,0}(\omega)g^{(0)}_{1,1}(\omega)-g^{(0)}_{0,1}(\omega)g^{(0)}_{1,0}(\omega)\big]}{N(\omega)},\\ N(\omega) &= 1-\varepsilon_0^* g^{(0)}_{0,0}(\omega)-2t_0^* g^{(0)}_{1,0}(\omega)-\varepsilon_1^* g^{(0)}_{1,1}(\omega)\\ &\quad +[\varepsilon_0^*\varepsilon_1^*-(t_0^*)^2]F(\omega),\\ F(\omega) &= g^{(0)}_{0,0}(\omega)g^{(0)}_{1,1}(\omega)-g^{(0)}_{1,0}(\omega)g^{(0)}_{0,1}(\omega).\end{aligned}\quad (84)$$

One can show that[20]

$$\begin{aligned}g^{(0)}_{1,1}(\omega) &= g^{(0)}_{0,0}(\omega)+\bar{t}^2\big[g^{(0)}_{0,0}(\omega)\big]^3,\\ \bar{t}^2F(\omega) &= \bar{t}\,g^{(0)}_{1,0}(\omega) = \big[\bar{t}\,g^{(0)}_{0,0}(\omega)\big]^2,\end{aligned}\quad (85)$$

so that we can cast our final third-order result into the form

$$\begin{aligned}g_{0,0}(\omega) &= \frac{g^{(0)}_{0,0}(\omega)-\varepsilon_1^*\big[g^{(0)}_{0,0}(\omega)\big]^2}{R(\omega)},\\ R(\omega) &= 1-(\varepsilon_0^*+\varepsilon_1^*)g^{(0)}_{0,0}(\omega)-\varepsilon_1^*\bar{t}^2\big[g^{(0)}_{0,0}(\omega)\big]^3\\ &\quad +(\varepsilon_0^*\varepsilon_1^*-(t_0^*)^2-2t_0^*\bar{t})\big[g^{(0)}_{0,0}(\omega)\big]^2.\end{aligned}\quad (86)$$

The density of states is the imaginary part of this expression, $2\pi D_{\rm LHB}(\omega) = \mathrm{Im}\,[g_{00}(\omega)]$. The bare boundary Green function is given by [$x=(\omega+U/2-\bar{\epsilon})/(2\bar{t})$],

$$\begin{aligned}\bar{t}\,g^{(0)}_{0,0}(\omega) &= \Theta(x^2-1)[x-\mathrm{sgn}(x)\sqrt{x^2-1}]\\ &\quad +\Theta(1-x^2)[x+\mathrm{i}\sqrt{1-x^2}],\end{aligned}\quad (87)$$

where $\Theta(x)$ is the Heaviside step function. For the density of states, we only need the region $|x|\leqslant 1$.

In Fig. 2, we show the results for the density of states of the LHB for $U=5$ (bandwidth $W=4$) for first, second, and third order in $1/U$. The overall spectra display a redshift of the Hubbard semiellipse (10), which describes the density of states for leading order $2D^{(0)}_{\rm LHB}(\omega)=\rho(\omega+U/2)$. The spectra for higher orders differ from each other mostly by a shift in the

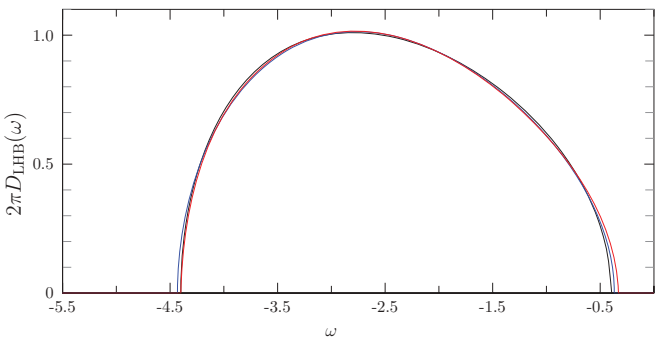


FIG. 2. (Color online) Density of states of the LHB, $2\pi D^{[n]}_{\rm LHB}(\omega)$, for $U=5$ (bandwidth $W=4$) up to and including orders $n=1,2,3$ (black, blue, and red colors).

spectral support so that the deviations are best visible close to the band edges.

#### *4. Band part of the Green function*

The full solution (84) contains higher-order corrections in $1/U$ due to the interaction dependence of the denominator $N(\omega)$. We may expand it order by order to derive a Taylor series in $1/U$ for the Green function. Such an order-by-order expansion ignores the fact that the attractive potential $\hat{W}$ generates resonance contributions at the band edges of the Hubbard band; see the following. Therefore, we denote the Green function from the order-by-order expansion as a band-part Green function. It can be cast into the form

$$\begin{aligned} 2\bar{t}G^{\text{band}}_{\text{LHB}}(\omega) &= \sum_{n=0}^{3}\lambda_n[\widetilde{g}_n(x)+g_n(x)],\\ 2\left(1+\frac{3}{8U^2}\right)x &= \omega+\frac{U}{2}-\frac{1}{2U}-\frac{35}{8U^3},\\ \widetilde{g}_n(|x|\geqslant 1) &= [T_{n+1}(x)-\text{sgn}(x)\sqrt{x^2-1}U_n(x)],\\ g_n(|x|\leqslant 1) &= [T_{n+1}(x)+\text{i}\sqrt{1-x^2}U_n(x)], \end{aligned} \tag{88}$$

with $T_n(x)$ [$U_n(x)$] as the Chebyshev polynomials of the first [second] kind,[33] and

$$\begin{aligned} \lambda_0 &= 1, \quad \lambda_1 = -\frac{1}{2U}-\frac{39}{16U^3},\\ \lambda_2 &= -\frac{1}{4U^2}, \quad \lambda_3 = -\frac{1}{8U^3} \end{aligned} \tag{89}$$

are the expansion coefficients. The first-order result was derived earlier in Ref. 28. Using an intuitive method, Eastwood[6] derived the band-part Green function for second order in $1/U$ for the Hubbard model in infinite dimensions. So far, their method could not be extended systematically to higher orders.

In Fig. 3, we show the resonance contribution to the density of states, $D^{\text{res}}_{\text{LHB}}(\omega)$ for $U = 5.5$. It is defined as the difference among the band part (88), $D^{\text{band}}_{\text{LHB}}(\omega)$, and the full density of states $D_{\text{LHB}}(\omega)$ (86). The difference is seen to be fairly small, which had to be expected because the potential $\hat{W}$ is rather weak. In general, the resonance contributions slightly increase the density of states close to the band edges and decrease it in the middle of the band.

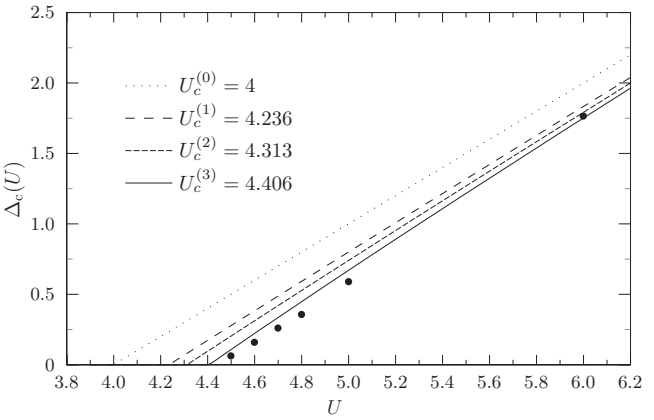


FIG. 4. Charge gap as a function of the interaction strength for various orders in the $1/U$ expansion. The dots are DDMRG data points.[8]

### B. Comparison with numerical results

Finally, we compare our analytical results with data from advanced numerical methods for the DMFT for the Mott-Hubbard insulator. The DDMRG method provides the gap and the density of states at zero temperature.[8] QMC gives the Matsubara-Green function at low but finite temperatures. Reference 6 contains a comparison with early methods in the field.

#### *1. Gap*

In Fig. 4. we show the gap as a function of the interaction strength for various orders in the $1/U$ expansion together with the DDMRG data of Ref. 8. The third-order theory reproduces the DDMRG data points very well.

Note, however, that in another DDMRG study,[9] the gap closes around $U = 4.8$. The differences in the two approaches lie in the reconstruction of the density of states and the extrapolation of the gap from the finite-size data. Apparently, different reconstruction algorithms can result in substantially different extrapolations close to the transition.

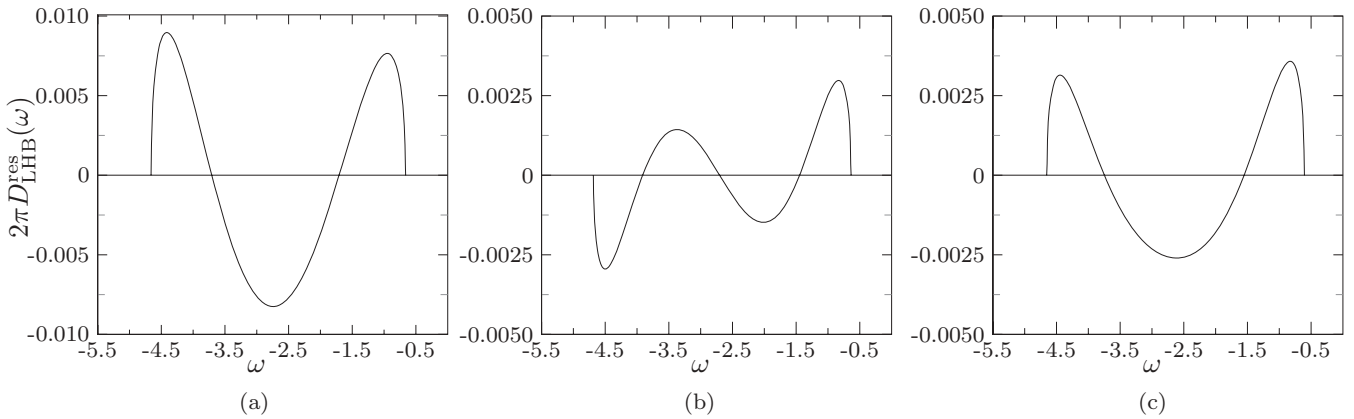


FIG. 3. Resonance contribution to the density of states of the LHB, $D^{\text{res}}_{\text{LHB}}(\omega) = D_{\text{LHB}}(\omega) - D^{\text{band}}_{\text{LHB}}(\omega)$, as a function of frequency in $n$th-order perturbation theory for $U = 5.5$ (bandwidth $W = 4$) (a) $n = 1$, (b) $n = 2$, (c) $n = 3$.

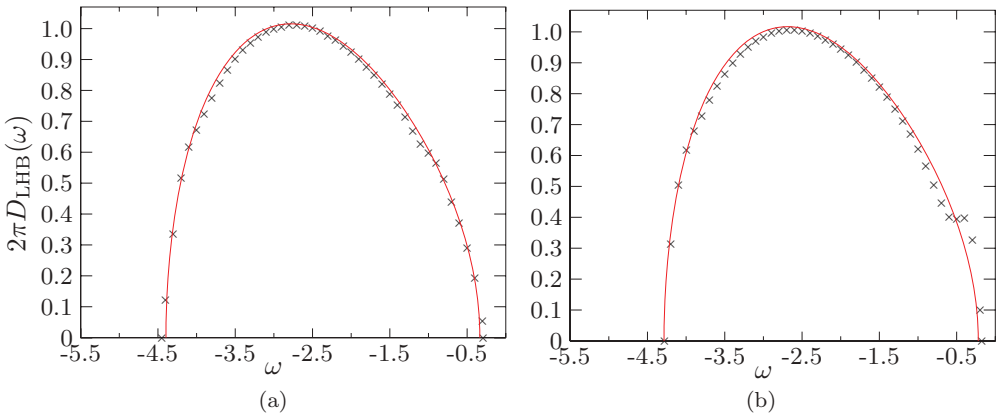


FIG. 5. (Color online) Density of states of the LHB from third-order perturbation theory in $1/U$ (full line) in comparison with DDMRG data points[8] for (a) $U = 5$ and (b) $U = 4.8$.

### 2. LHB

In Fig. 5, we show the density of states for $U = 4.8$ at third order in $1/U$ together with the DDMRG data of Ref. 8. The overall agreement is very good. This has already been observed from the results for second order.[6]

It is seen that a resonance develops at the upper band edge in the DDMRG data, which is not seen in perturbation theory for third order. For $U = 4.5$, the resonance is more pronounced[8] and resembles the split quasiparticle peak of the metallic phase. One may wonder whether such a resonance could be obtained from higher-order perturbation theory. A model study[32] shows that the parameter set $\varepsilon_0^* = -0.2$ and $\varepsilon_{1\leqslant m\leqslant 9}^* = 0.1/m$ in the scattering potential $\hat{W}$ can readily account for both the overall redshift of the density of states and a resonance at the upper band edge. Since the range of the repulsive potential is finite, an expansion of the density of states to high but finite order could possibly reproduce the resonance seen in the DDMRG data.

### 3. Matsubara-Green function

The Matsubara-Green function for the Hubbard model is defined by

$$\mathcal{G}(\tau) = -\frac{1}{L}\sum_i \mathrm{Tr}\,[e^{\beta(\Omega-\hat{H})}\mathcal{T}_\tau \hat{c}_{i,\sigma}(\tau)\hat{c}_{i,\sigma}^\dagger(0)], \tag{90}$$

where $\beta = 1/k_B T$ is the inverse temperature, $\Omega$ is the grand-canonical potential, and $\mathcal{T}_\tau$ orders the operators in imaginary time. The operators in imaginary-time Heisenberg representation are defined by $(-\beta \leqslant \tau \leqslant \beta)$

$$\hat{c}_{i,\sigma}(\tau) = e^{\tau\hat{H}}\hat{c}_{i,\sigma}e^{-\tau\hat{H}}, \quad \hat{c}_{i,\sigma}^\dagger(\tau) = e^{\tau\hat{H}}\hat{c}_{i,\sigma}^\dagger e^{-\tau\hat{H}}. \tag{91}$$

The Fourier transformation of the Matsubara-Green function is defined on the points $\mathrm{i}\omega_n = (2n+1)\pi/\beta$ ($n$: integer) on the imaginary axis.

The retarded Green function at finite temperature $T$ is obtained from the analytic continuation,

$$G_{\mathrm{ret}}(\omega;\beta) = \mathcal{G}(\mathrm{i}\omega_n \to \omega + \mathrm{i}\eta). \tag{92}$$

Therefore, we may express the Matsubara-Green function with the help of the density of states at finite temperature in the form

$$\mathcal{G}(\tau) = \int_{-\infty}^{\infty} d\omega \left[\frac{\mathrm{Im}\,[G_{\mathrm{ret}}(\omega;\beta)]}{\pi}\right]\frac{e^{-\omega\tau}}{e^{-\beta\omega}+1}, \tag{93}$$

with $0 \leqslant \tau \leqslant \beta$. Note that it is easy to evaluate Eq. (93) for a given density of states, but it is very difficult to reconstruct the density of states from numerical data for $\mathcal{G}(\tau)$.

For very low temperatures and for large interaction strengths, we approximate the density of states by its zero-temperature expression for third order,

$$\mathcal{G}(\tau) \approx -\int_{-\infty}^{\infty} d\omega\,[D_{\mathrm{LHB}}(\omega) + D_{\mathrm{LHB}}(-\omega)]\frac{e^{-\omega\tau}}{e^{-\beta\omega}+1}, \tag{94}$$

which we compare with QMC data of Blümer.[34] The approximation is not as drastic as it may seem because, deep in the Mott-Hubbard insulator, thermal excitations are exponentially suppressed due to the finite charge gap. Therefore, corrections to Eq. (94) should be exponentially small in $\Delta_c(U)/k_B T$.

In Figs. 6 and 7, we compare our analytical results, Eq. (94), to QMC data for $\beta = 20$ ($T = 0.05$) at $U = 6$ and $U = 5.2$, where the gaps are $\Delta_c(U = 6) = 1.75$ and $\Delta_c(U = 5.2) = 0.89$, respectively. The results agree very well. Note, however, that $\mathcal{G}(\tau)$ is rather featureless so that fine points, such as the

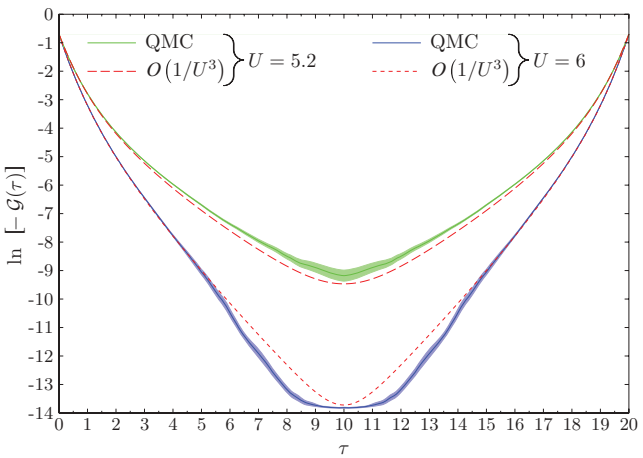


FIG. 6. (Color online) Third-order result and QMC data for the Matsubara-Green function for $U = 6$ (blue) and $U = 5.2$ (green). The inverse temperature is $\beta = 20$ ($T = 0.05$), the gaps are $\Delta_c(U = 6) = 1.75$ and $\Delta_c(U = 5.2) = 0.89$, respectively. Note that the data are shown on a logarithmic scale. The shading indicates the statistical error in the QMC data.

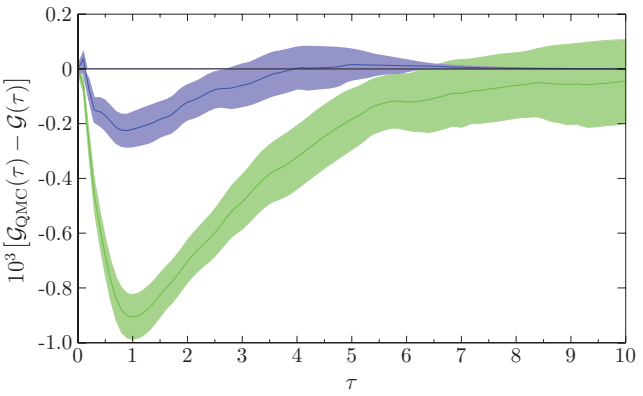


FIG. 7. (Color online) Difference between the third-order result and QMC data for the Matsubara-Green function for $U = 6$ (blue) and $U = 5.2$ (green). The inverse temperature is $\beta = 20$ ($T = 0.05$); the gaps are $\Delta_c(U = 6) = 1.75$ and $\Delta_c(U = 5.2) = 0.89$, respectively. Note that the difference is augmented by a factor of $10^3$ to make it visible. The shading indicates the statistical error in the QMC data.

width of the Hubbard bands or the density of states cannot be reconstructed easily from QMC data for $\mathcal{G}(\tau)$.

## VI. CONCLUSIONS

In this paper, we have studied the Mott-Hubbard insulating phase of the Hubbard model on a Bethe lattice with an infinite coordination number. We have adopted the Kato-Takahashi perturbation theory to solve the self-consistency equation of the DMFT analytically for the symmetric SIAM in perturbation theory up to and including third order in the inverse coupling strength $U$. To this end, it has been necessary to use the mapping of the SIAM from the star geometry onto the two-chain geometry, which represents the energetically separated LHB and UHB. In higher orders, a multichain mapping is required in order to resolve the various Hubbard sub-bands. For the present paper, we could ignore the secondary Hubbard bands whose weight is of fourth order in $1/U$.

We confirm earlier analytical results[6] for the Mott-Hubbard gap at second order on a Bethe lattice with an infinite coordination number and extend them to third order systematically. The agreement between the perturbation theory in $1/U$ and the DDMRG data of Ref. 8 for the gap is very good. Note, however, that the precise value of the critical interaction $U_c$, where the gap closes, and the analytical behavior of the gap, as a function of $U$ close to the transition, are still under debate.[9]

The previous paper[6] provides the Green function as a Taylor expansion in $1/U$, whereas the present paper includes resonance corrections. The full density of states results from the calculation of the boundary Green function for a particle on a semi-infinite chain with nearest-neighbor electron transfers and an attractive interaction near the boundary, whose parameters we derived for third order in $1/U$. For all interaction strengths where perturbation theory is applicable, $U \gtrsim 5$ (bandwidth $W = 4$, $4.4 \lesssim U_c \lesssim 4.8$), the resonance contributions are small.

For $U \gtrsim 5$, the agreement between the analytical results for the density of states and the DDMRG data[8] is very good for all frequencies. In addition, our zero-temperature expressions for the density of states provides a very good approximation for the density of states at small but finite temperatures. This can be seen from the excellent agreement between our approximate Matsubara-Green function and QMC data.[34]

As in all kinds of perturbation theories, the number of terms to be calculated rapidly increases with the index of the order. In principle, the fourth-order terms could still be calculated by hand. This requires a four-chain geometry so that the secondary Hubbard sub-bands can be treated properly. For fourth order, there are more than 30 terms in the Kato-Takahashi operator and in the projected Hamiltonian. According to our analysis, much higher orders are needed to reproduce a resonance feature seen in the DDMRG data[8] at the upper band edge of the LHB. Such high-order calculations for the density of states appear to be forbiddingly costly within the DMFT.

The ground-state energy of the Hubbard model on a Bethe lattice with an infinite coordination number was calculated for high orders using a computer algorithm based on the Kato-Takahashi expansion.[35] In the future, we plan to devise a similar algorithm for the calculation of the Mott-Hubbard gap. With a high-order expansion for the Mott-Hubbard gap, we should be able to locate $U_c$ with much better accuracy.

Our approach can be extended to multiband Hubbard models on a Bethe lattice. Apparently, in the strong-coupling limit, each band must be mapped onto two separate chains in the SIAM in order to represent the UHB and LHB. It would be desirable to provide analytical results in the strong-coupling limit as tests for numerical approaches to the DMFT for multiband Hubbard models.

## ACKNOWLEDGMENTS

We thank Marlene Nahrgang for her contributions to the early stages of this paper and Jörg Bünemann for useful discussions.

[1] A. Georges, G. Kotliar, W. Krauth, and M. J. Rozenberg, Rev. Mod. Phys. **68**, 13 (1996).
[2] W. Metzner and D. Vollhardt, Phys. Rev. Lett. **62**, 324 (1989).
[3] R. Bulla, Phys. Rev. Lett. **83**, 136 (1999); see R. Bulla, T. Costi, and T. Pruschke, Rev. Mod. Phys. **80**, 395 (2008).
[4] M. Caffarel and W. Krauth, Phys. Rev. Lett. **72**, 1545 (1994); Y. Ōno, R. Bulla, A. C. Hewson, and M. Potthoff, Eur. Phys. J. B **22**, 283 (2001).
[5] Q. Si, M. J. Rozenberg, G. Kotliar, and A. E. Ruckenstein, Phys. Rev. Lett. **72**, 2761 (1994).
[6] M. P. Eastwood, F. Gebhard, E. Kalinowski, S. Nishimoto, and R. M. Noack, Eur. Phys. J. B **35**, 155 (2003).
[7] R. M. Noack and F. Gebhard, Phys. Rev. Lett. **82**, 1915 (1999); S. Ejima, F. Gebhard, and R. M. Noack, Eur. Phys. J. B **66**, 191 (2008).
[8] S. Nishimoto, F. Gebhard, and E. Jeckelmann, J. Phys. Condens. Matter **16**, 7063 (2004).

[9]M. Karski, C. Raas, and G. S. Uhrig, Phys. Rev. B **72**, 113110 (2005).
[10]M. Jarrell, Phys. Rev. Lett. **69**, 168 (1992).
[11]N. Blümer, Phys. Rev. B **76**, 205120 (2007).
[12]A. N. Rubtsov, V. V. Savkin, and A. I. Lichtenstein, Phys. Rev. B **72**, 035122 (2005); P. Werner, A. Comanac, L. de Medici, M. Troyer, and A. J. Millis, Phys. Rev. Lett. **97**, 076405 (2006).
[13]M. J. Rozenberg, G. Kotliar, and X. Y. Zhang, Phys. Rev. B **49**, 10181 (1994).
[14]D. E. Logan, M. P. Eastwood, and M. A. Tusch, J. Phys. Condens. Matter **9**, 4211 (1997).
[15]M. Potthoff, Eur. Phys. J. B **36**, 335 (2003).
[16]F. Gebhard, E. Jeckelmann, S. Mahlert, S. Nishimoto, and R. M. Noack, Eur. Phys. J. B **36**, 491 (2003).
[17]D. Ruhl and F. Gebhard, J. Stat. Mech. Exp. Theor. (2006) P03015.
[18]T. Kato, Prog. Theor. Phys. **4**, 514 (1949).
[19]M. Takahashi, J. Phys. C **10**, 1289 (1977).
[20]D. Ruhl, Ph.D. thesis, Marburg, 2010; available electronically as [http://archiv.ub.uni-marburg.de/diss/z2010/0377/pdf/ddfr.pdf].
[21]R. J. Baxter, *Exactly Solved Models in Statistical Mechanics* (Dover, New York, 2007).
[22]A. L. Fetter and J. D. Walecka, *Quantum Theory of Many-Particle Systems* (Dover, New York, 2003).
[23]M. Eckstein, M. Kollar, K. Byczuk, and D. Vollhardt, Phys. Rev. B **71**, 235119 (2005).
[24]See A. C. Hewson, *The Kondo Problem to Heavy Fermions* (Cambridge University Press, Cambridge, UK, 1993).
[25]D. E. Logan, M. P. Eastwood, and M. A. Tusch, J. Phys. Condens. Matter **10**, 2673 (1998); M. R. Galpin and D. E. Logan, Eur. Phys. J. B **62**, 129 (2008).
[26]E. H. Lieb and F. Y. Wu, Phys. Rev. Lett. **20**, 1445 (1968).
[27]N. F. Mott, *Metal Insulator Transitions* (Taylor and Francis, London, 1974, 1990); F. Gebhard, *The Mott Metal Insulator Transition* (Springer, Berlin, 1997).
[28]For a first application of this idea, see M. Nahrgang, M.Sc. thesis, Marburg, 2008.
[29]M. J. Rozenberg, G. Möller, and G. Kotliar, Mod. Phys. Lett. **8**, 535 (1994).
[30]W. Metzner, P. Schmit, and D. Vollhardt, Phys. Rev. B **45**, 2237 (1992).
[31]E. N. Economou, *Green's Functions in Quantum Physics*, Springer Series in Solid-State Sciences, Vol. 7 (Springer, Berlin, 1979), Chap. 6.
[32]M. Hoyer, B. Sc. thesis, Marburg, 2010.
[33]M. Abramovitz and I. A. Stegun, *Handbook of Mathematical Functions* (Dover, New York, 1970).
[34]N. Blümer (private communication).
[35]N. Blümer and E. Kalinowski, Phys. Rev. B **71**, 195102 (2005).